

RSC Advances



This is an *Accepted Manuscript*, which has been through the Royal Society of Chemistry peer review process and has been accepted for publication.

Accepted Manuscripts are published online shortly after acceptance, before technical editing, formatting and proof reading. Using this free service, authors can make their results available to the community, in citable form, before we publish the edited article. This *Accepted Manuscript* will be replaced by the edited, formatted and paginated article as soon as this is available.

You can find more information about *Accepted Manuscripts* in the [Information for Authors](#).

Please note that technical editing may introduce minor changes to the text and/or graphics, which may alter content. The journal's standard [Terms & Conditions](#) and the [Ethical guidelines](#) still apply. In no event shall the Royal Society of Chemistry be held responsible for any errors or omissions in this *Accepted Manuscript* or any consequences arising from the use of any information it contains.

Molten salt synthesis of nano-sized $\text{Li}_4\text{Ti}_5\text{O}_{12}$ doped with Fe_2O_3 as anode materials for lithium-ion battery

Qingjun Guo, Shiyun Li, Heng Wang, Yuan Gao, Bing Li*

East China University of Science and Technology, 130 Meilong Road, Shanghai, 200237

Abstract: A single phase $\text{Li}_4\text{Ti}_{5-x}\text{Fe}_x\text{O}_{12}$ ($x=0, 0.1, 0.2, 0.3$) with spinel structure has been synthesized in LiCl-KCl molten salts with a stoichiometric molar ratio of $\text{LiOH}\cdot\text{H}_2\text{O}$, TiO_2 , Fe_2O_3 , LiCl-KCl of 4:5:x/2:20 ($x=0, 0.1, 0.2, 0.3$). The effects of Fe_2O_3 on the phase structure, morphology and particle size of $\text{Li}_4\text{Ti}_5\text{O}_{12}$ were characterized by X-ray diffraction (XRD), scanning electron microscope (SEM) and transmission electron microscope (TEM) equipped with energy dispersive spectroscope (EDS). The electrochemical performances of the $\text{Li}_4\text{Ti}_{5-x}\text{Fe}_x\text{O}_{12}$ ($x=0, 0.1, 0.2, 0.3$) were characterized by charge-discharge curves, electrochemical impedance spectroscopy (EIS) and cyclic voltammetry (CV). The results show that Fe_2O_3 homogeneously distributes in the crystal lattice of $\text{Li}_4\text{Ti}_5\text{O}_{12}$ and make the lattice parameters slightly increase due to Fe^{3+} ions doping. Addition of 0.1 molar ratio Fe_2O_3 to $\text{Li}_4\text{Ti}_5\text{O}_{12}$ has reduced the particle size of $\text{Li}_4\text{Ti}_5\text{O}_{12}$ from 1 μm to about 200 nm. The obtained $\text{Li}_4\text{Ti}_{4.8}\text{Fe}_{0.2}\text{O}_{12}$ as anode material of Lithium-ion battery has presented the capacity of 173.7 mAhg^{-1} at 0.2 C, approach to the theoretical capacity of $\text{Li}_4\text{Ti}_5\text{O}_{12}$ (175 mAhg^{-1}), and given a capacity of 103.4 mAhg^{-1} at 10 C, much larger than the value of pure $\text{Li}_4\text{Ti}_5\text{O}_{12}$ (28.7 mAhg^{-1}). This is well explained by the EIS and CV results.

Keywords: Molten salt synthesis; Fe_2O_3 ; $\text{Li}_4\text{Ti}_5\text{O}_{12}$; lithium-ion battery

* Corresponding author.

E-mail address: bingli@ecust.edu.cn.

1. Introduction

The spinel $\text{Li}_4\text{Ti}_5\text{O}_{12}$ (LTO) has recently attracted much attention due to Zero Type Variational, high safety and good thermal stability as anode materials for Lithium-ion battery (LIB). However, the empty Ti 3d state with band energy of about 2eV causes LTO intrinsic low electronic and ionic conductivity, worse rate performance, which have limited its wide commercialization^{1,2}.

Therefore, several LTO modification methods such as coating carbon³ or metallic conducting layer on the surface⁴, doping ions⁵⁻¹³ in the position of Li, Ti or O, and reducing the particle size^{14, 15} have been proposed to improve the conductivity and rate performance of LTO. Ions doping can cause LTO lattice defect and make a rapid Li-ion intercalation/deintercalation processes. Reducing the particle size can shorten Li-ion transfer route and therefore improve the rate performance¹⁶.

LTO is usually synthesized by solid-state method, the synthesized LTO materials are usually composed of inhomogeneous, larger size particles with lower activity as the anode materials of LIBs. As a promising method, molten salts method has shown excellent advantages in controlling composition, morphology, activity and homogeneity of LTO because molten salts are homogenous media for the solid phase synthesis reaction and can realize molecule even atom level mixture for the reactants and prevent particles aggregation. Liang Cheng¹⁷ has reported that nano-scale LTO is synthesized in a mass of LiCl (the molar ratio of LiCl to TiO_2 is as high as 16) molten salt and has shown an initial capacity of 159 mAhg^{-1} as anode materials of LIB. Bai¹⁸ has mainly researched the influences of composite molten salts on the morphology and performances of synthesized spinel LTO.

Usually, during LTO molten salts synthesis process heterogeneous nuclei such as Fe_2O_3 rather than LTO is facilitated to reduce the particle size of LTO. Moreover, Fe_2O_3 itself is a potential anode material for LIB^{19,20}. Spinel LTO covered by a thin film of Fe_2O_3 , has been prepared by solid-state method combined with hydrolysis method and further 12 h heat-treatment²¹. The obtained $\text{Li}_4\text{Ti}_5\text{O}_{12}/\text{Fe}_2\text{O}_3$ composites as anode materials of LIB have showed a discharge capacity of 109.4 mAhg^{-1} at 10 C

and superior cycling stability with an initial discharge capacity of 145.3 mAhg^{-1} at 2 C rate. However, the fabrication process is very complicated and Fe_2O_3 has not doped into $\text{Li}_4\text{Ti}_5\text{O}_{12}$ crystal lattice.

Therefore, in this paper, molten salts method is used to directly synthesize nano-sized $\text{Li}_4\text{Ti}_{5-x}\text{Fe}_x\text{O}_{12}$ ($x=0, 0.1, 0.2, 0.3$) (LT(F)O) in LiCl-KCl molten salts with a stoichiometric molar ratio of $\text{LiOH}\cdot\text{H}_2\text{O}$, TiO_2 , Fe_2O_3 , LiCl-KCl of 4:5:x/2:20 ($x=0, 0.1, 0.2, 0.3$). The thimbleful amount of Fe_2O_3 is added to further reduce particle size and improve LTO electronic conductivity so as to improve its electrochemical performance as LIB. The effects of Fe_2O_3 on the morphology, structure and electrochemical performance of LTO are investigated.

2. Experimental

2.1. Preparation of LT(F)O

The raw materials used in the experiments include $\text{LiOH}\cdot\text{H}_2\text{O}$ (RG, Adamas Reagent, Ltd.), anatase TiO_2 (AR, XiyaReagent, Ltd), LiCl, KCl and Fe_2O_3 ($\geq 99.0\%$, AR, Sinopharm Chemical Reagent Co., Ltd), A stoichiometric molar ratio of $\text{LiOH}\cdot\text{H}_2\text{O}$, TiO_2 , Fe_2O_3 and LiCl-KCl of 4:5:x/2:20 ($x=0,0.1,0.2,0.3$) is weighed and mixed in an agate mortar for 10 min. Then the mixture is placed in a corundum crucible, rapidly heated to $800 \text{ }^\circ\text{C}$ and held for 4 h under air atmosphere. After naturally cooled to room temperature, the mixture is washed with deionized water and filtered repeatedly until the chloride ions could not be detected in AgNO_3 solution. The LT(F)O powders are obtained after drying at $120 \text{ }^\circ\text{C}$ for 12 h in a drying oven under air atmosphere.

2.2. Sample characterization

X-ray diffraction (XRD, D/max2550V) with Cu $K\alpha_1$ ($10^\circ < 2\theta < 80^\circ$) radiation is used to identify the phase composition and crystal lattice parameters of the prepared powders. Morphology and particle size of the powders are determined by scanning electron microscope (SEM, JEOL JSM-6360LV), and the nanoscale microstructure of the particles is examined using transmission electron microscope (TEM, JEM-2100)

equipped with energy dispersive spectroscopy (EDS, VARIO ELIII).

2.3. Electrochemical test

For electrochemical measurements, the LT(F)O electrodes are made by the following steps: homogenous slurries are prepared by mixing the solute comprising of obtained LT(F)O, carbon black (Super-P) and polyvinylidene fluoride (PVDF) (weight ratio of 80:10:10) with N-methyl-2-pyrrolidone (NMP) solvent (the weight ratio of solute and solvent is 1:3.86), and magnetically stirring for 4 h. Then the slurry is cast onto a copper foil to form a 100 μm thick film by a coating machine. The film is heated to 90 $^{\circ}\text{C}$ and remained for 12 h in a vacuum oven to evaporate the solvent. The copper foil is further cut into disks of diameter 12 mm by using mechanical drilling machine and pressed the electrode plates into 50 μm thickness using tableting machine. The total amounts of the electrode slices are selected as 11.5-13.5 mg, so the weight of LT(F)O sample electrodes are 2.0-3.0 mg. The coin-type cells with the prepared LT(F)O slices as the anode and lithium plate ($\Phi 16\text{ mm} \times 1.5\text{ mm}$, China Energy Lithium Co., Ltd.) as the cathode in a 1 M LiPF_6 in ethylene carbonate (EC), dimethyl carbonate (DMC) and ethyl methyl carbonate (EMC) (1:1:1 in volume) electrolyte with a Celgard 2400 separator are assembled in an argon-filled glove box, both the contents of H_2O and O_2 are less than 1 ppm.

All the electrochemical tests are carried out in a two-electrode system in which LT(F)O electrode is used as the working electrode, lithium plate as the counter and reference electrodes. During cycle tests, the coin cells are charged/discharged under different current densities by designating cut-off voltages of 1.2 V and 2.5 V vs. Li/Li^+ by using a charge/discharge battery tester (New ware TC5.X, Shenzhen). The cyclic voltammetry (CV) and electrochemical impedance spectroscopy (EIS) are measured by electrochemical workstation (Parstat 2237). The scan rate of CV is 0.1 mV/s in the potential range of 0 to 3 V, and the EIS is measured at 5 mV amplitude with the frequency from 100 kHz to 0.01 Hz.

It is worth to note that in the paper the charge indicates Li intercalation into LT(F)O electrode and the discharge means Li deintercalation from the LT(F)O electrode.

3. Results and discussion

3.1. XRD results

The XRD patterns of LT(F)O are shown in Fig. 1a. All the samples show the major diffraction peaks which are in accordance with spinel LTO (JCPDS Card No.49-0207), indicating that the crystal structure of LTO is retained after Fe₂O₃ modification. However, as Fe₂O₃ molar ratio increases from 0 to 0.15, the diffraction peaks of (111) plane shift to higher diffraction angles in Fig. 1b, and the lattice parameters of LTO increase from 0.8354 nm to 0.8365 nm in table 1. The results imply that some Fe³⁺ ions doped into the crystal lattice and substitute Ti⁴⁺ ions position and make the lattice parameters slightly increase even though Fe³⁺ ion (0.064 nm) is a little smaller than Ti⁴⁺ ion (0.067 nm). This is could be explained as follows. When the smaller trivalent iron ion took the 16d site where the lithium ions located, the lithium ions could randomly occupy the 8a, 16c or 48f sites to provide the charge compensation for the iron ion that lead to the increase lattice parameter so that the paths for Li⁺ ion intercalation/deintercalation become widen^{22,23}.

Fig. 1. XRD pattern of as-prepared Li₄Ti_{5-x}Fe_xO₁₂ (x=0,0.1,0.2,0.3).

Table 1

The lattice parameter of LT(F)O.

3.2. SEM and TEM analysis

SEM images of the LT(F)O samples are shown in Fig. 2a-d. The four samples are well crystallized with uniform particle size distribution. The particle size obviously decreases as Fe₂O₃ molar ratio increases from 0 to 0.15. The pure LTO particle size is around 0.5-1.5 μm, Li₄Ti_{4.7}Fe_{0.3}O₁₂ and Li₄Ti_{4.8}Fe_{0.2}O₁₂ are around 150-250 nm. The results demonstrate that a small amount of Fe₂O₃ doping into LTO has significantly reduced the particle size and the specific surface area of LTO²⁴. The reason why LTO doped with Fe₂O₃ can reduce the particle size of LTO will be discussed in the future.

Fig. 2. SEM images of $\text{Li}_4\text{Ti}_{5-x}\text{Fe}_x\text{O}_{12}$ (a) $x=0$; (b) $x=0.1$; (c) $x=0.2$; (d) $x=0.3$.

Fig. 3. TEM images of $\text{Li}_4\text{Ti}_{4.8}\text{Fe}_{0.2}\text{O}_{12}$ with energy dispersive spectroscopy (EDS) (a) the smooth surface; (b) the roughened surface.

Fig. 4. TEM image of $\text{Li}_4\text{Ti}_{4.8}\text{Fe}_{0.2}\text{O}_{12}$ and the corresponding EDX mapping images of Fe, O and Ti elements.

Fig. 5. HRTEM image of $\text{Li}_4\text{Ti}_{4.8}\text{Fe}_{0.2}\text{O}_{12}$ powder.

TEM images in Fig. 3 show that the surface of $\text{Li}_4\text{Ti}_{4.8}\text{Fe}_{0.2}\text{O}_{12}$ exists some small bumps in some sites. Element composition on both the smooth surface in Fig. 3a and the roughened surface (with bumps) in Fig. 3b by the energy dispersive spectroscopy (EDS) has shown almost the same Ti, O and Fe elements. Further study by the energy dispersive X-ray (EDX) mapping in Fig. 4 has shown that Fe element uniformly distributes in the whole particle as the Ti and O elements, suggesting that the small bumps are also subsize LTO crystal grains and Fe elements homogeneously distribute in the crystal lattice of LTO. The morphology and internal structure of $\text{Li}_4\text{Ti}_{4.8}\text{Fe}_{0.2}\text{O}_{12}$ are further characterized by transmission electron microscopy (TEM) and high-resolution transmission electron microscopy (HRTEM). The clear lattice fringes of $\text{Li}_4\text{Ti}_{4.8}\text{Fe}_{0.2}\text{O}_{12}$ obtained by HRTEM images in Fig. 5 indicate that $\text{Li}_4\text{Ti}_{4.8}\text{Fe}_{0.2}\text{O}_{12}$ has a well-defined crystal structure. The d-spacing 0.244 nm of the particle matches with that of (222) plane of spinel LTO²⁵.

3.3. Electrochemical performances

In order to characterize the effects of Fe_2O_3 on LT(F)O cyclic performance as anode materials for LIB, the first charge/discharge curves and cycling performance of LT(F)O between 1.2 and 2.5 V at 0.2 C rate are measured and shown in Fig. 6.

From the first charge/discharge curves in Fig. 6a, all the samples show a flat voltage plateau around 1.5-1.6 V (vs. Li/Li^+), which corresponds to the result of the

reversible phase transition between $\text{Li}_4\text{Ti}_5\text{O}_{12}$ and $\text{Li}_7\text{Ti}_5\text{O}_{12}$ during Li-ion intercalation/deintercalation processes²⁶. The first charge/discharge capacities of $\text{Li}_4\text{Ti}_{5-x}\text{Fe}_x\text{O}_{12}$ ($x=0, 0.1, 0.2, 0.3$) electrodes are $156.3 \text{ mAhg}^{-1}/132.5 \text{ mAhg}^{-1}$ ($x=0$), $166.6 \text{ mAhg}^{-1}/140.66 \text{ mAhg}^{-1}$ ($x=0.1$), $173.7 \text{ mAhg}^{-1}/149.8 \text{ mAhg}^{-1}$ ($x=0.2$) and $169.3 \text{ mAhg}^{-1}/140.4 \text{ mAhg}^{-1}$ ($x=0.3$), respectively. Obviously, pure LTO sample presents the lowest first charge/discharge capacity and the shortest flat plateau profile than LTFO, and $\text{Li}_4\text{Ti}_{4.8}\text{Fe}_{0.2}\text{O}_{12}$ sample shows the biggest charge capacity of 173.7 mAhg^{-1} among all the samples, approach to the theoretical capacity of LTO (175 mAhg^{-1}). The performance improvement demonstrates advantage of transition metal oxides Fe_2O_3 doping in LTO²⁷.

From the cycling performance and coulombic efficiency curves in Fig. 6b-c, pure LTO discharge capacity fades and fluctuates seriously, while LTFO electrodes present excellent cycling stability at 0.2 C rate. Therefore, Fe_2O_3 doped LTO demonstrates much better electrochemical performance than pure LTO. The average coulombic efficiencies of $\text{Li}_4\text{Ti}_{5-x}\text{Fe}_x\text{O}_{12}$ ($x=0, 0.1, 0.2, 0.3$) electrodes excluding the first lower coulombic efficiencies, in Fig. 6c are 97.5%, 98.7%, 99.2%, 98.9% at 50 cycles at 0.2 C rate, respectively. The lower first coulombic efficiencies, is attributed to the large irreversible capacity in the first discharge/charge cycle mainly caused by lithium adsorption in the carbon black^{28,29} and some lithium ions occupation of 8a sites which cannot be extracted electrochemically^{30,31}.

Fig. 6d shows the rate capabilities of LT(F)O electrodes at different C-rates, in which C-rates are calculated according to the theoretical capacity of LTO (175 mAhg^{-1}). Specific charge capacity gradually decreases with C-rates increasing. Three samples of $\text{Li}_4\text{Ti}_{5-x}\text{Fe}_x\text{O}_{12}$ ($x=0.1, 0.2, 0.3$) (LTFO) have shown better rate performance and higher capacity at each same rate than that of pure LTO. $\text{Li}_4\text{Ti}_{4.8}\text{Fe}_{0.2}\text{O}_{12}$ electrode presents the largest charge capacity of 173.7 mAhg^{-1} (0.2 C), 139.2 mAhg^{-1} (0.6 C), 132.4 mAhg^{-1} (1.3 C), 123.1 mAhg^{-1} (3 C) and 103.4 mAhg^{-1} (10 C). Especially, $\text{Li}_4\text{Ti}_{4.8}\text{Fe}_{0.2}\text{O}_{12}$ electrode gives 103.4 mAhg^{-1} at 10 C, much larger than 25 mAhg^{-1} of pure LTO. Though the charge capacity of $\text{Li}_4\text{Ti}_{5-x}\text{Fe}_x\text{O}_{12}$ ($x=0.1, 0.3$) (140.7 mAhg^{-1} , 142.7 mAhg^{-1} , respectively) at 0.6 C is

relatively higher than that of $\text{Li}_4\text{Ti}_{4.8}\text{Fe}_{0.2}\text{O}_{12}$, $\text{Li}_4\text{Ti}_{4.8}\text{Fe}_{0.2}\text{O}_{12}$ is much more stable at every rate and shows excellent performances at high rate. Hence, Fe_2O_3 doped has significantly improved rate performance and stability of LTO. Especially, $\text{Li}_4\text{Ti}_{4.8}\text{Fe}_{0.2}\text{O}_{12}$ has shown the best electrochemical performance.

Fig. 6. (a) First charge/discharge curves; (b) specific charge capacities at 0.2 C for 50 cycles; (c) coulombic efficiency of $\text{Li}_4\text{Ti}_{5-x}\text{Fe}_x\text{O}_{12}$ ($x=0,0.1,0.2,0.3$) at 0.2 C rate between 1.2 and 2.5 V (versus Li/Li^+) and (d) the rate capabilities of charge at different rates.

Fig. 7. (a) Electrochemical impedance spectra (EIS) of $\text{Li}_4\text{Ti}_{5-x}\text{Fe}_x\text{O}_{12}$ ($x=0,0.1,0.2,0.3$) at electrodes at open circuit potential with the simulation equivalent curves; (b) the simulation equivalent circuit for the EIS.

Table 2

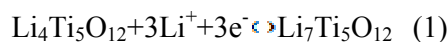
Result of EIS analysis of LT(F)O electrodes.

Electrochemical impedance spectra (EIS) of LT(F)O are also measured on the coin cells after 50 charge and discharge cycles with the simulation equivalent curves by using ZsimpWin software in Fig.7a and the simulation equivalent circuit is also obtained in Fig. 7b. All the EIS curves consist of a small semi circle in high frequency region and a sloping line in low frequency region. The real axis intercept R_s of impedance spectroscopy in the high frequency region corresponds to electrolyte resistance, ohmic resistance including electrode resistances, contact resistances, ect. The diameter values for the semi circle of the spectra correspond to charge transfer resistance (R_{ct}) of the electrochemical reaction^{32, 33}. The sloping line also named as Warburg impedance represents lithium ions diffusion resistance in the LT(F)O electrode materials. The charge transfer resistance (R_{ct}) and the Warburg diffuse resistance of LTFO are lower than that of pure LTO, especially the ohmic resistance R_s and the charge transfer resistance R_{ct} of $\text{Li}_4\text{Ti}_{4.8}\text{Fe}_{0.2}\text{O}_{12}$ electrode are the smallest ones (4.49 Ω , 25.38 Ω) among the samples. In the outermost shell 4s state of iron

atom has two electrons which easy to lose. It contributes additional electrons and provides electronic carriers for the conduction band³⁴. Thereby, LTFO show higher electronic conductivity than pure LTO. As a consequence, the higher electrical conductivity of LTFO decreases the charge transfer resistance of anode materials³⁵. This is favorable for Li⁺ intercalation/deintercalation into the anodes.

Fig. 8. Cyclic voltammograms of Li₄Ti_{5-x}Fe_xO₁₂ (x=0,0.1,0.2,0.3) electrodes in a 1M LiPF₆ in ethylene carbonate (EC), dimethyl carbonate (DMC) and ethyl methyl carbonate (EMC) (1:1:1 in volume) electrolyte with scan rate of 0.1 mV/s. WE: LT(F)O electrodes (1.13 cm²), CE and RE: Li foil (2.01 cm²).

After 50 charge and discharge cycles the cyclic voltammograms (CVs) of LT(F)O electrodes are obtained at the scan rate of 0.1 mV/s shown in Fig. 8. All the CV curves have a pair of reduction peak at about 1.45 V and oxidation peak at about 1.75 V, which represents lithium ions intercalation/deintercalation accompanying successive oxidation/reduction reactions of the Ti³⁺/Ti⁴⁺ couple in LT(F)O electrode materials³⁶ and can be presented as below³⁷:



LTFO electrodes have shown larger reduction currents and oxidation currents than pure LTO electrode in Fig. 8. Especially, Li₄Ti_{4.8}Fe_{0.2}O₁₂ electrode not only has presented the largest reduction/oxidation current, but also given a smaller potential difference of 0.37 V between the oxidation and reduction peaks than that of the pure LTO electrode of 0.5 V. A smaller potential difference has indicated that Fe₂O₃ doped LTO not only reduces anode polarization to some extent which significantly improves the rate performance. Such behavior coincides with the above results of cycling performance, rate capabilities and EIS analysis.

In addition, another reduction peak at about 0.55 V occurred in pure LTO electrode is caused by Li ions further intercalation into LTO electrode, and can be presented as below³⁷:



LTFO electrodes hardly have shown the reduction peak at 0.55 V in the Fig. 8. and all the oxidation/reduction reactions are fulfilled between 1.2-2.5 V. This implies that the reduction reaction for Li ions at 0.55 V shifts to more positive potential occurred for the equation (1) due to more wide and random paths for Li ions intercalation/deintercalation in LTFO electrodes resulted from Fe₂O₃ doping as mentioned above.

The electrochemical performance for LTFO electrode is dependent on both the particle size and Fe₂O₃ content. All the LTFO electrodes have shown smaller particle size to ensure a larger contact area between anode material and electrolyte, hence shortened the Li ions diffusion paths and improved the electrochemical reaction rate³⁸. Simultaneously, Fe₂O₃ doping into LTO has increased the lattice parameters of LTO, which helps to speed up Li ions diffusion rate in the crystal lattice. But Fe³⁺ ions also can occupy certain positions in the crystal lattice and more Fe³⁺ ions will impede Li ions diffusion rate in the crystal lattice. So a proper Fe₂O₃ doping level in LTO can achieve the best electrochemical property. In the present work, as x=0.2 in Li₄Ti_{5-x}Fe_xO₁₂, that is, Li₄Ti_{4.8}Fe_{0.2}O₁₂ sample has shown the largest capacity, the best rate performance together with cyclic stability. Therefore, Li₄Ti_{4.8}Fe_{0.2}O₁₂ material by molten salts method will likely spur LTO wide commercialized for lithium ion batteries.

4. Conclusions

A single phase Li₄Ti_{5-x}Fe_xO₁₂ (x=0,0.1,0.2,0.3) (LT(F)O) with spinel structure are successfully synthesized in LiCl-KCl molten salts containing a stoichiometric molar ratio of LiOH·H₂O, TiO₂ and Fe₂O₃. The results show that Fe₂O₃ homogenously distributes in the crystal lattice of LTO and make the lattice parameters slightly increase by Fe³⁺ ions intercalation. Among the three samples, addition of 0.1 molar ratio Fe₂O₃ to LTO has effectively reduced the particle size of pure LTO from 1 μm to about 200 nm. And the formed Li₄Ti_{4.8}Fe_{0.2}O₁₂ as an anode material of LIB has presented the largest capacity of 173.7 mAhg⁻¹ at 0.2 C, approach to the theoretical

capacity of LTO (175 mAhg^{-1}), and given a capacity of 103.4 mAhg^{-1} at 10 C, much larger than the value of pure LTO (28.7 mAhg^{-1}). Besides, all the samples exhibit above 95% coulombic efficiencies after 50 cycles at 0.2 C rate. $\text{Li}_4\text{Ti}_{4.8}\text{Fe}_{0.2}\text{O}_{12}$ sample has presented the smallest the ohmic resistance R_s and the charge transfer resistance R_{ct} ($4.49 \ \Omega$, $25.38 \ \Omega$) among the samples. Meantime, $\text{Li}_4\text{Ti}_{4.8}\text{Fe}_{0.2}\text{O}_{12}$ electrode not only has presented the largest reduction/oxidation current, but also the given a smaller potential difference of 0.37 V between the oxidation and reduction peaks than that of the pure LTO electrode of 0.5 V. Therefore, $\text{Li}_4\text{Ti}_{4.8}\text{Fe}_{0.2}\text{O}_{12}$ electrode reduces the anode polarization to some extent but also significantly improves the electrochemical activity. All the results have demonstrate that addition Fe_2O_3 could restrain LTO particle growth in molten salts, and the Fe_2O_3 modified LTO delivers a higher discharge capacity, high rate capacity and better long-term cycling stability.

Acknowledgement

This work was financially supported by National Natural Science Foundation of China (No. 51474107).

References

- 1 C. Y. Ouyang, Z. Y. Zhong, M. S. Lei, *Electrochem. Commun.*, 2007, **9**, 1107-1112.
- 2 T. Brousse, P. Fragnaud, R. Marchand, D. M. Schleich, O. Bohnke, K. West, *J. Power Sources*, 1997, **68**, 412-415.
- 3 G. D. Du, B. R. Winton, I. M. Hashim, N. Sharma, K. Konstantinov, M. V. Reddy, Z. P. Guo, *RSC Adv.*, 2014, **4**, 38568-38574.
- 4 S. H. Huang, Z. Y. Wen, J. C. Zhang, X. L. Yang, *Electrochim Acta*, 2007, **52**, 3704-3708.
- 5 M. Krajewski, M. Michalska, B. Hamankiewicz, D. Ziolkowska, K. P. Korona, J. B. Jasinski, M. Kaminska, L. Lipinska, A. Czerwinski, *J. Power Sources*, 2014, **245**, 764-771.

- 6 D. Capsoni, M. Bini, V. Massaritti, P. Mustarelli, S. Ferrari, G. Chiodelli, M.C. Mozzati, P. Galinetto, *J. Phys Chem C.*, 2009, **113**, 19664-19671.
- 7 S. H. Huang, Z. Y. Wen, X. J. Zhu, Z. H. Gu, *J. Electrochem. Commun.*, 2004, **11**, 1093-1097.
- 8 C. H. Chen, J. T. Vaughey, A. N. Jansen, D. W. Dees, A. J. Kahaian, T. Goacher, M. M. Thackeray, *J. Electrochem. Soc.*, 2001, **148**, A102-A104.
- 9 Z. Wang, G. Chen, J. Xu, Z. Lv, W. Yang, *J. Phys. Chem. Solids*, 2011, **72**, 773-778.
- 10 S. H. Huang, Z. Y. Wen, X. J. Zhu, Z. X. Lin, *J. Power Sources*, 2007, **165**, 408-412.
- 11 B. B. Tian, H. F. Xiang, L. Zhang, Z. Li, H. H. Wang, *Electrochim. Acta*, 2010, **55**, 5453-5458.
- 12 J. Wolfenstine, J. L. Allen, *J. Power Sources*, 2008, **180**, 582-585.
- 13 Y. Qi, Y. Huang, D. Jia, S. J. Bao, Z. P. Guo, *Electrochim. Acta*, 2009, **54**, 4772-4776.
- 14 H. Yan, Z. Zhu, D. Zhang, W. Li, *J. Power Sources*, 2012, **219**, 45-51.
- 15 F. X. Wu, X. H. Li, Z. X. Wang, H. J. Guo, Z. J. He, Q. Zhang, X. H. Xiong, P. Yue, *J. Power Sources*, 2012, **202**, 374-379.
- 16 S. M. Venkate, C. H. Chen, J. S. Do, C. W. Lin, T. C. Chou, B. J. Hwang, *J. Power Sources*, 2005, **146**, 204-208.
- 17 L. Cheng, H. J. Liu, J. J. Zhang, H. M. Xiong, Y. Y. Xia, *J. Electrochem Soc.*, 2006, **153**, A1472-A1477.
- 18 Y. Bai, F. Wang, F. Wu, C. Wu, L. Y. Bao, *Electrochim Acta*, 2008, **54**, 322-327.
- 19 Y. Z. Jiang, D. Zhang, Y. Li, T. Z. Yuan, N. Bahlawane, C. Liang, W. P. Sun, Y. H. Lu, M. Yan, *Nano Energy*, 2014, **4**, 23-30.
- 20, M. Chen, W. Li, X. Shen, G. W. Diao, *ACS applied materials & interfaces*, 2014, **6**, 4514-4523.
- 21 B. Wang, J. Cao, Y. Liu, T. Zeng, L. Li, *J. alloys and compounds*, 2013, **587**, 21-25.
- 22 Z. Zhao, Y. L. Xu, M. D. Ji, H. Zhang. *Electrochim. Acta*, 2013, **109**, 645-650.

- 23 K. Y. Li, H. Chen, F. F. Shua, D. F. Xue, X. W. Guo, RSC Adv., 2014, **4**, 36507-36512.
- 24 J. Li, Y. L. Jin, X. G. Zhang, H. Yang, Solid State Ionics, 2007, **178**, 1590-1594.
- 25 Y. B. He, M. Liu, Z. D. Huang, B. Zhang, Y. Yu, B. H. Li, F.Y. Kang, J. K. Kim, J. Power Sources, 2013, **239**, 269-276.
- 26 D. Wang, C. M. Zhang, Y. Y. Zhang, J. Wang, D. N. He, Ceramics International, 2013, **39**, 5145-5149.
- 27 X. F. Li, C. L. Wang, J. Mater. Chem. A, 2013, **1**, 165-182.
- 28 W. J. H. Borghols, M. Wagemaker, U. Lafont, E. M. Kelder, F. M. Mulder, J. Am. Chem. Soc., 2009, **131**, 17786-17792.
- 29 X. L. Yao, S. Xie, H. Q. Nian, C. H. Chen, J. Alloys Compd., 2008, **465**, 375-379.
- 30 Y. R. Jhan, C. Y. Lin, J. G. Duh, Mater. Lett. 2011, **65**, 2502-2505.
- 31 J. Shu, J. Solid State Electrochem., 2009, **13**, 1535-1539.
- 32 J. M. Tarascon, M. Armand, Nature, 2001, **414**, 359-367.
- 33 J. J. Huang, Z. Y. Jiang, Electrochim. Acta, 2008, **53**, 7756-7759.
- 34 X. F. Li, J. Liu, Y. Zhang, Y. L. Li, H. Liu, X. B. Meng, J. L. Yang, D. S. Geng, D. N. Wang, R. Y. Li, X. L. Sun, J. Power Sources, 2012, **197**, 238-245.
- 35 G. Liu, H. Zheng, A. S. Simens, A. M. Minor, X. Song, V. S. Battaglia, J. Electrochem. Soc., 2007, **154**, A1129-A1134.
- 36 T. F. Yi, Y. Xie, Q. J. Wu, J. Power Sources, 2012, **214**, 220-226.
- 37 F. T. Yi, Y. Xie, Y. R. Zhu, R. S. Zhu, H. Y. Shen, J. Power Sources, 2013, **222**, 448-454.
- 38 X. F. Li, A. Dhanabalan, C. L. Wang, J. Power Sources, 2011, **196**, 9625-9630.

LIST OF TABLE AND FIGURE CAPTIONS

Table 1 The lattice parameter of LT(F)O.

Table 2 Result of EIS analysis of LT(F)O electrodes.

Fig. 1. XRD pattern of as-prepared $\text{Li}_4\text{Ti}_{5-x}\text{Fe}_x\text{O}_{12}$ ($x=0,0.1,0.2,0.3$).

Fig. 2. SEM images of $\text{Li}_4\text{Ti}_{5-x}\text{Fe}_x\text{O}_{12}$ (a) $x=0$; (b) $x=0.1$; (c) $x=0.2$; (d) $x=0.3$.

Fig. 3. TEM images of $\text{Li}_4\text{Ti}_{4.8}\text{Fe}_{0.2}\text{O}_{12}$ with energy dispersive spectroscopy (EDS) (a) the smooth surface; (b) the roughened surface.

Fig. 4. TEM image of $\text{Li}_4\text{Ti}_{4.8}\text{Fe}_{0.2}\text{O}_{12}$ and the corresponding EDX mapping images of Fe, O and Ti elements.

Fig. 5. HRTEM image of $\text{Li}_4\text{Ti}_{4.8}\text{Fe}_{0.2}\text{O}_{12}$ powder.

Fig. 6. (a) First charge/discharge curves; (b) specific charge capacities for 50 cycles; (c) coulombic efficiency of $\text{Li}_4\text{Ti}_{5-x}\text{Fe}_x\text{O}_{12}$ ($x=0,0.1,0.2,0.3$) at 0.2 C rate between 1.2 and 2.5 V (versus Li/Li^+) and (d) the rate capabilities of charge at different rates.

Fig. 7. (a) Electrochemical impedance spectra (EIS) of $\text{Li}_4\text{Ti}_{5-x}\text{Fe}_x\text{O}_{12}$ ($x=0,0.1,0.2,0.3$) at electrodes at open circuit potential with the simulation equivalent curves; (b) the simulation equivalent circuit for the EIS.

Fig. 8. Cyclic voltammograms of $\text{Li}_4\text{Ti}_{5-x}\text{Fe}_x\text{O}_{12}$ ($x=0,0.1,0.2,0.3$) electrodes in a 1M LiPF_6 in ethylene carbonate (EC), dimethyl carbonate (DMC) and ethyl methyl carbonate (EMC) (1:1:1 in volume) electrolyte with scan rate of 0.1 mV/s. WE: LT(F)O electrodes (1.13 cm^2), CE and RE: Li foil (2.01 cm^2).

Table 1**The lattice parameter of LT(F)O.**

Sample	α (nm)
Li ₄ Ti ₅ O ₁₂	0.8354
Li ₄ Ti _{4.9} Fe _{0.1} O ₁₂	0.8364
Li ₄ Ti _{4.8} Fe _{0.2} O ₁₂	0.8365
Li ₄ Ti _{4.7} Fe _{0.3} O ₁₂	0.8365

Table 2**Result of EIS analysis of LT(F)O electrodes.**

Sample	Rs/ Ω	Rct/ Ω	Capacitance/F	W/ $\Omega^{-1}s^{-1}$
Li ₄ Ti ₅ O ₁₂	13.43	88.32	3.219×10^{-6}	0.003979
Li ₄ Ti _{4.9} Fe _{0.1} O ₁₂	12.17	36.45	3.922×10^{-6}	0.001014
Li ₄ Ti _{4.8} Fe _{0.2} O ₁₂	4.498	25.38	6.242×10^{-6}	0.001365
Li ₄ Ti _{4.7} Fe _{0.3} O ₁₂	11.95	59.48	4.681×10^{-6}	0.001621

Rs, the ohmic resistance, ect; Rct, charge transfer resistance; W, Warburg diffusion impedance

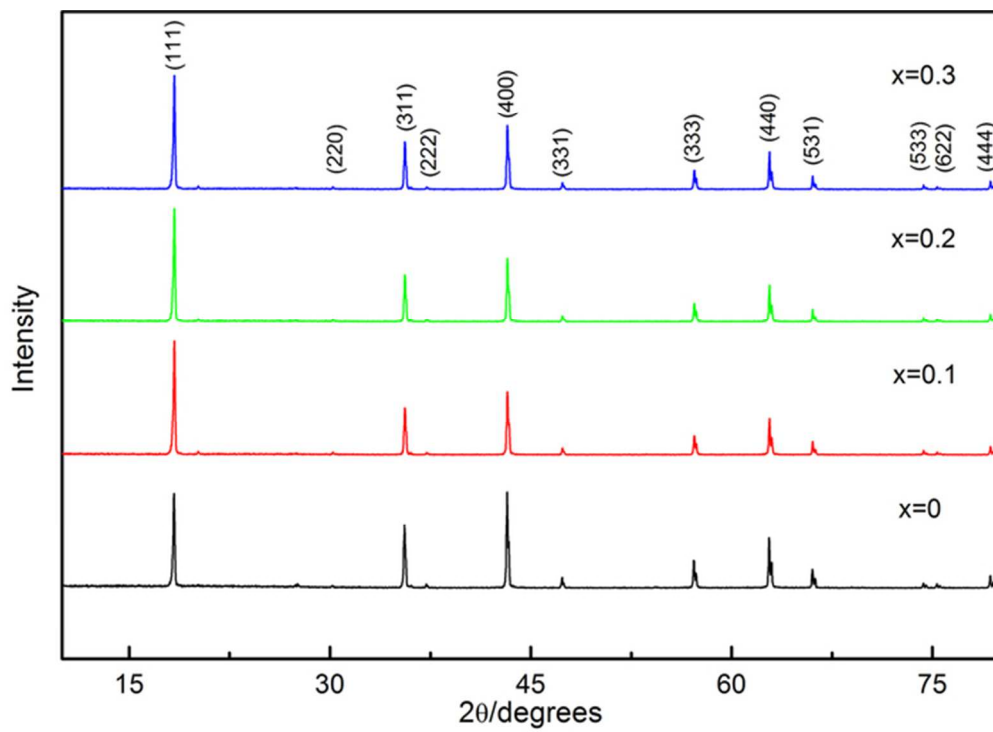


Fig. 1. XRD pattern of as-prepared $\text{Li}_4\text{Ti}_5-x\text{Fe}_x\text{O}_{12}$ ($x=0,0.1,0.2,0.3$).
59x43mm (300 x 300 DPI)

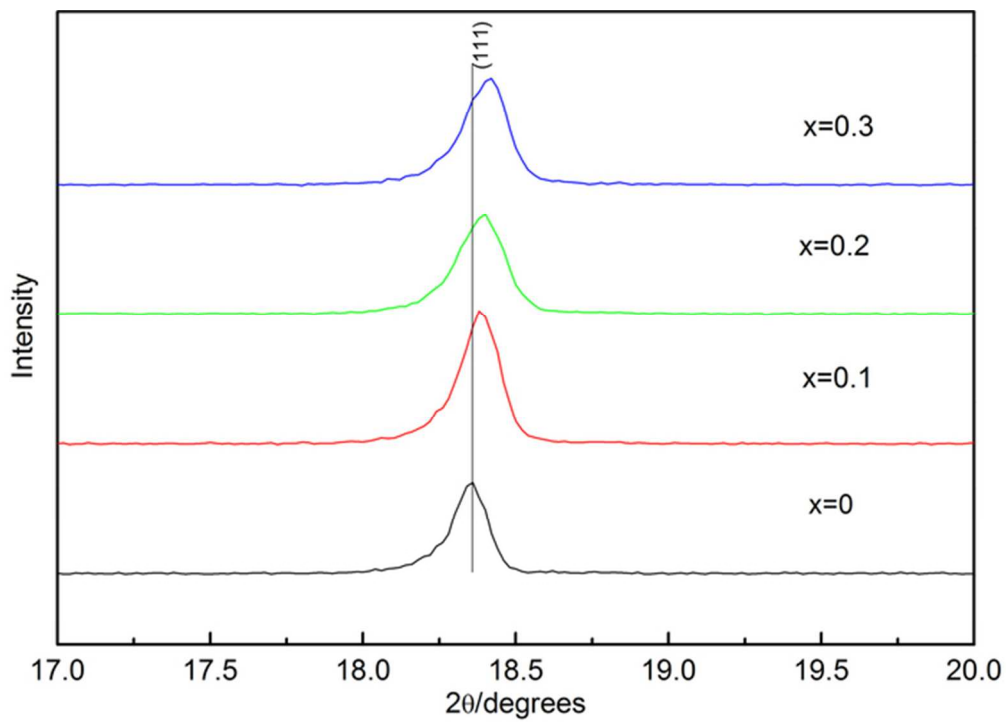


Fig. 1. XRD pattern of as-prepared $\text{Li}_4\text{Ti}_5\text{-xFe}_x\text{O}_{12}$ ($x=0,0.1,0.2,0.3$).
59x41mm (300 x 300 DPI)

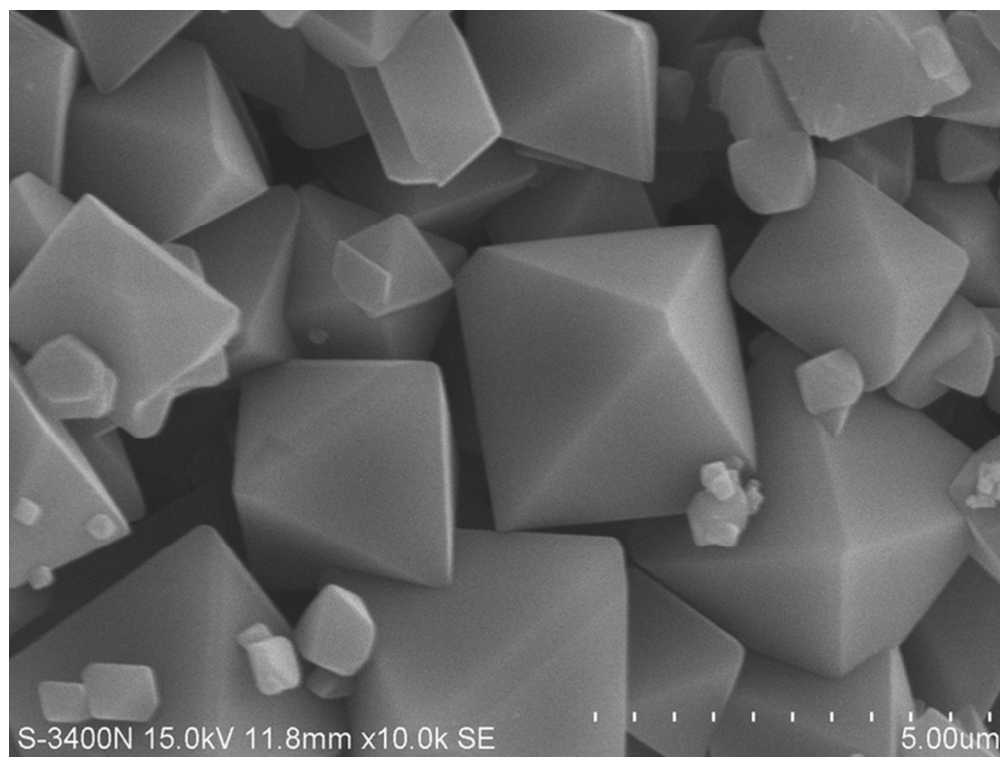


Fig. 2. SEM images of Li₄Ti_{5-x}Fe_xO₁₂ (a) x = 0.
62x46mm (300 x 300 DPI)

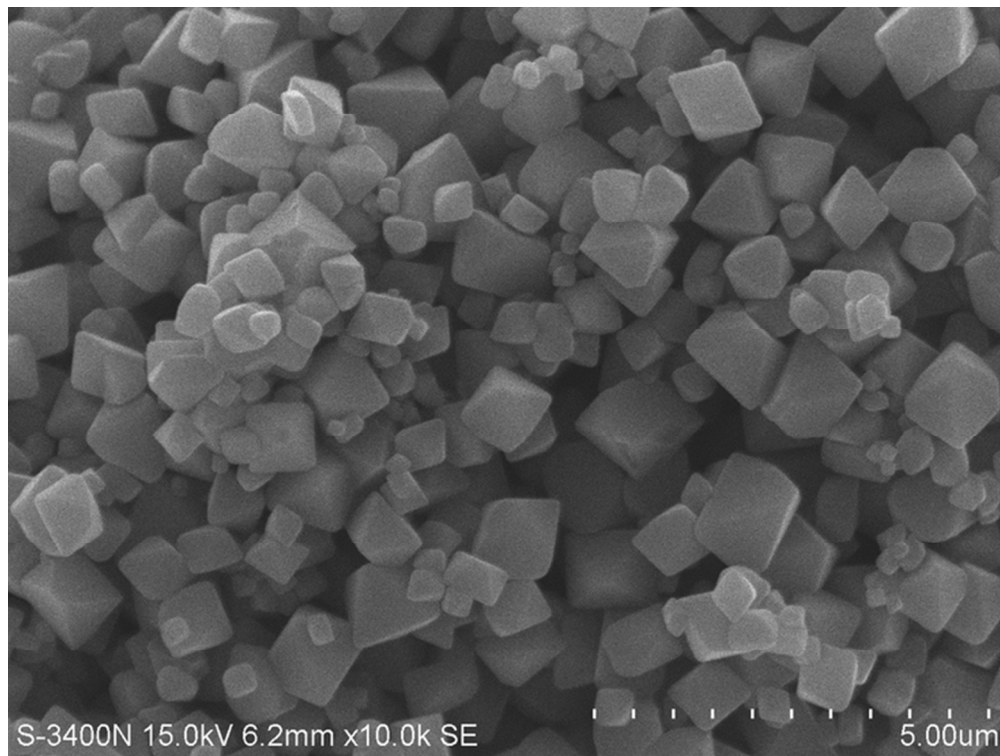


Fig. 2. SEM images of $\text{Li}_4\text{Ti}_5\text{-xFe}_x\text{O}_{12}$ (b) $x = 0.1$.
62x46mm (300 x 300 DPI)

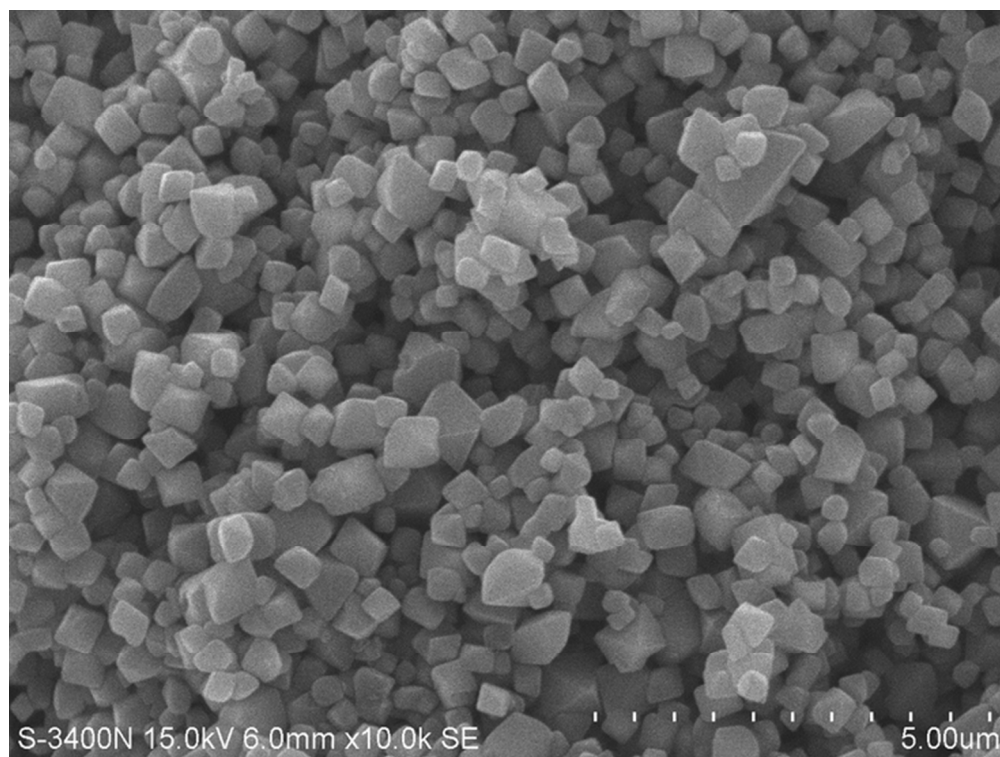


Fig. 2. SEM images of Li₄Ti_{5-x}Fe_xO₁₂ (c)x = 0.2.
62x46mm (300 x 300 DPI)

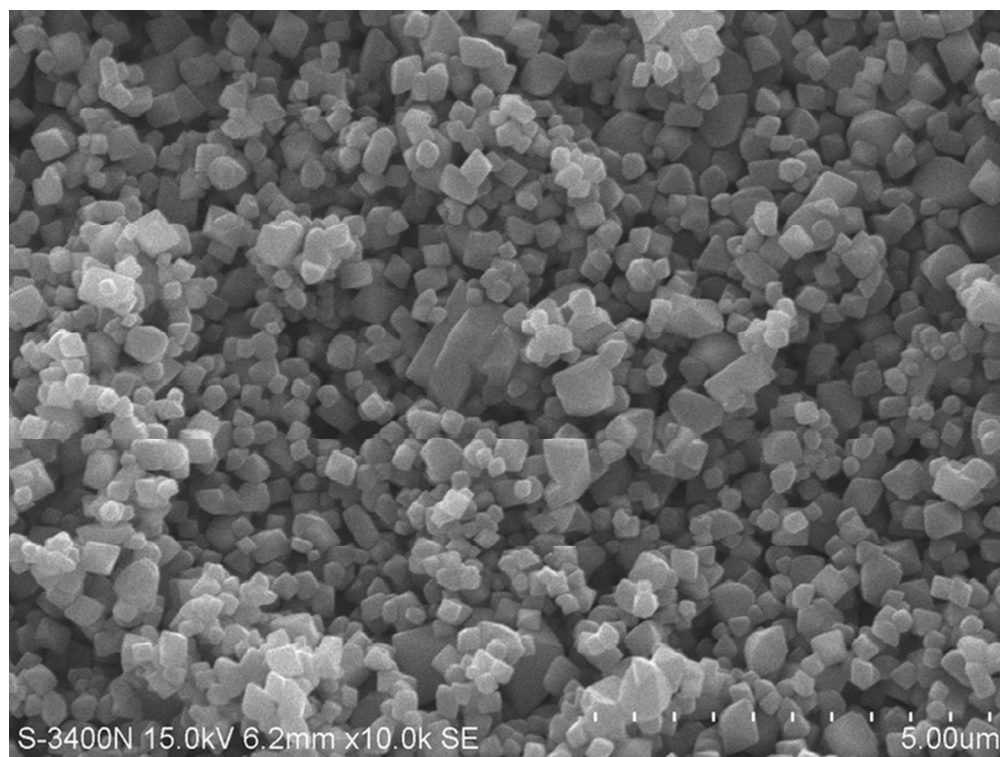


Fig. 2. SEM images of $\text{Li}_4\text{Ti}_5\text{-xFe}_x\text{O}_{12}$ (d) $x=0.3$.
62x46mm (300 x 300 DPI)

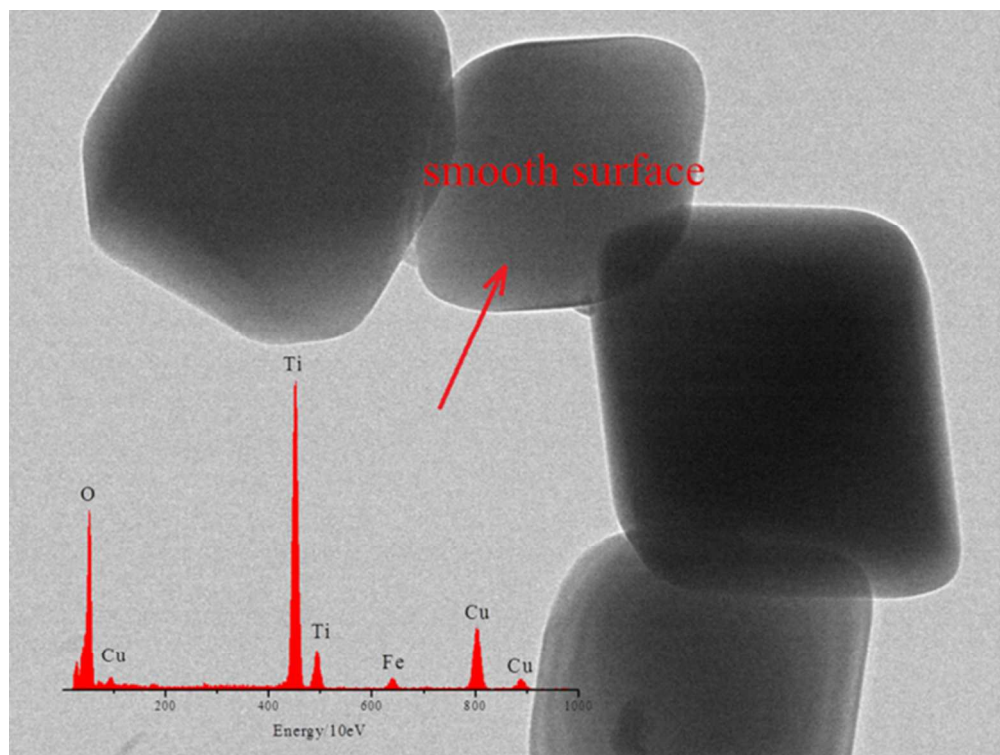


Fig. 3. TEM images of $\text{Li}_4\text{Ti}_4.8\text{Fe}_{0.2}\text{O}_{12}$ with energy dispersive spectroscopy (EDS) (a) the smooth surface. 62x46mm (300 x 300 DPI)

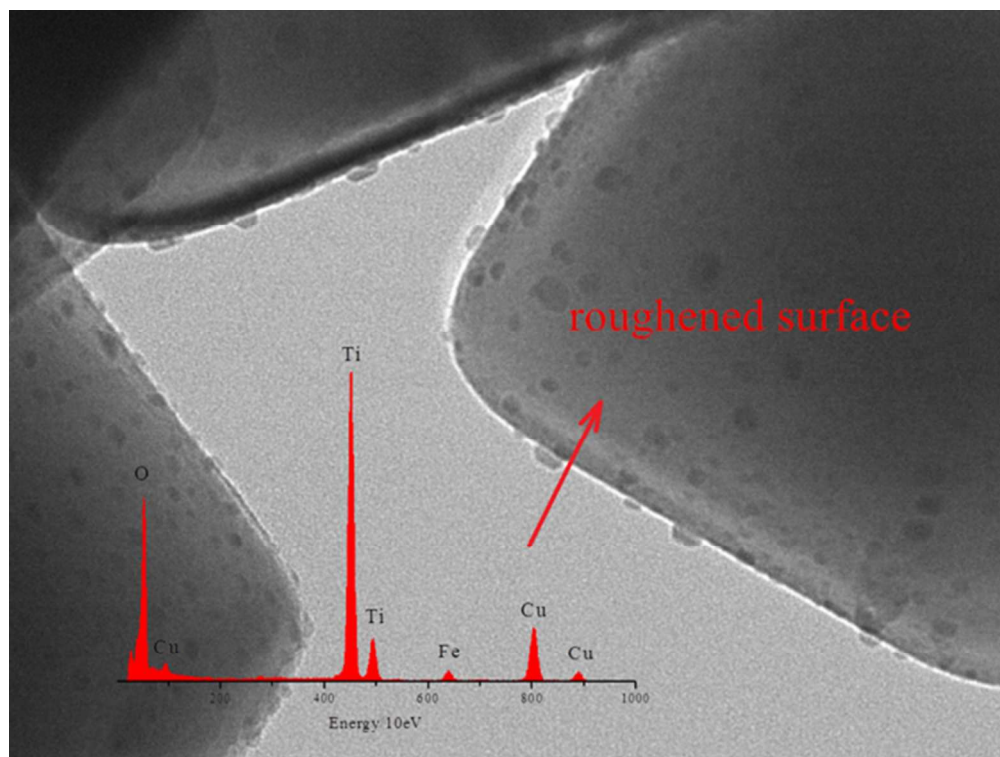


Fig. 3. TEM images of $\text{Li}_4\text{Ti}_4.8\text{Fe}_{0.2}\text{O}_{12}$ with energy dispersive spectroscopy (EDS) (b) the roughened surface.
62x46mm (300 x 300 DPI)

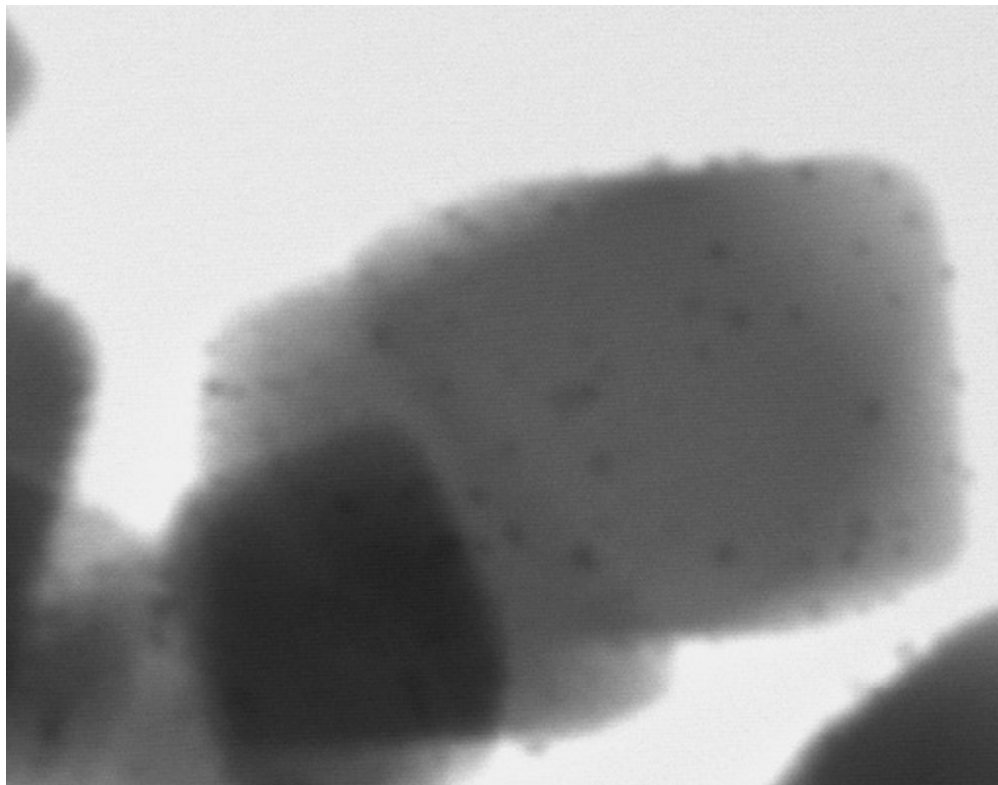


Fig. 4. TEM image of Li₄Ti_{4.8}Fe_{0.2}O₁₂ and the corresponding EDX mapping images of Fe, O and Ti elements.
64x50mm (300 x 300 DPI)



Fig. 4. TEM image of $\text{Li}_4\text{Ti}_{4.8}\text{Fe}_{0.2}\text{O}_{12}$ and the corresponding EDX mapping images of Fe, O and Ti elements.
64x50mm (300 x 300 DPI)

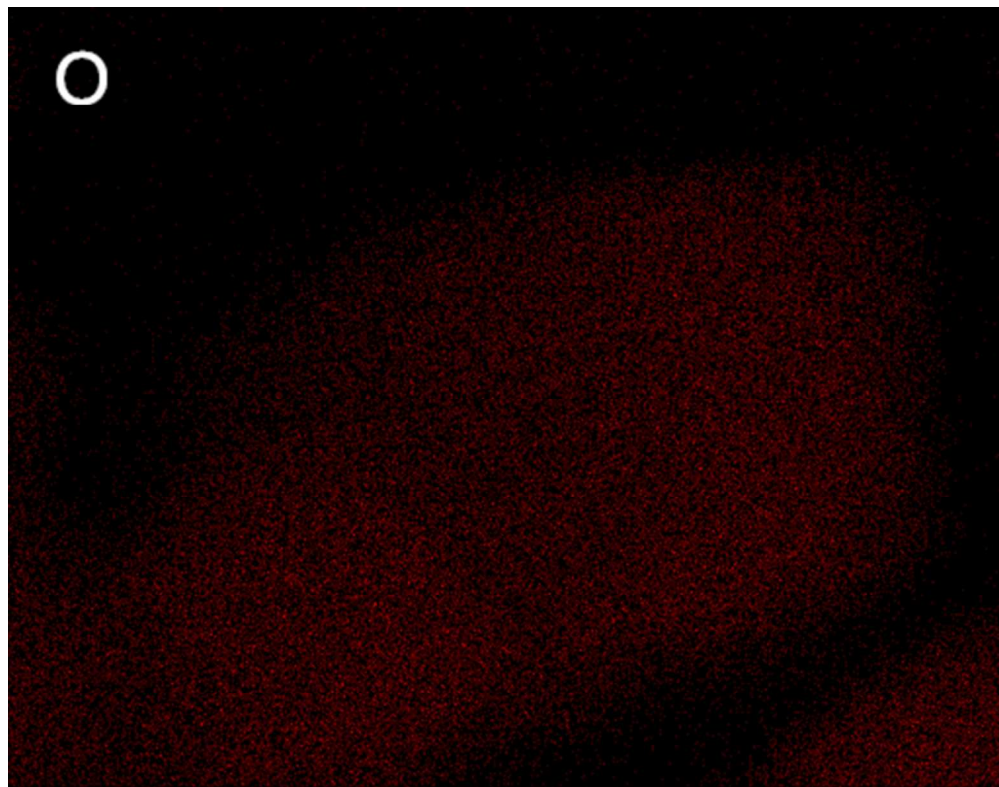


Fig. 4. TEM image of $\text{Li}_4\text{Ti}_{4.8}\text{Fe}_{0.2}\text{O}_{12}$ and the corresponding EDX mapping images of Fe, O and Ti elements.
64x50mm (300 x 300 DPI)

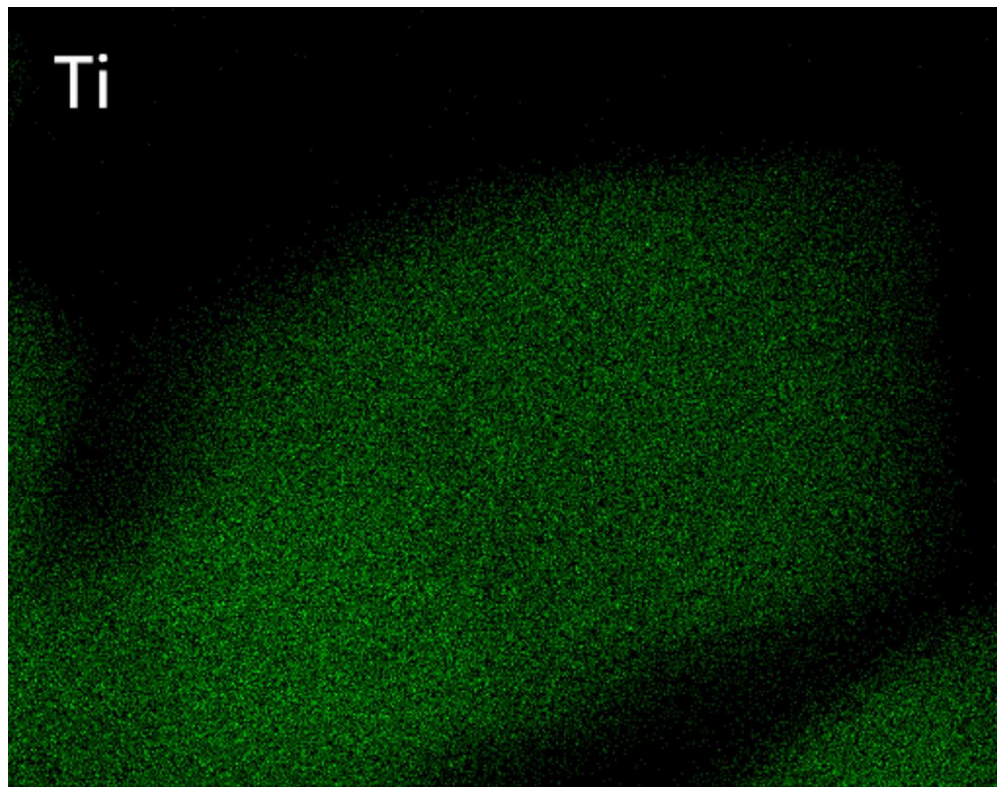


Fig. 4. TEM image of $\text{Li}_4\text{Ti}_{4.8}\text{Fe}_{0.2}\text{O}_{12}$ and the corresponding EDX mapping images of Fe, O and Ti elements.
64x50mm (300 x 300 DPI)

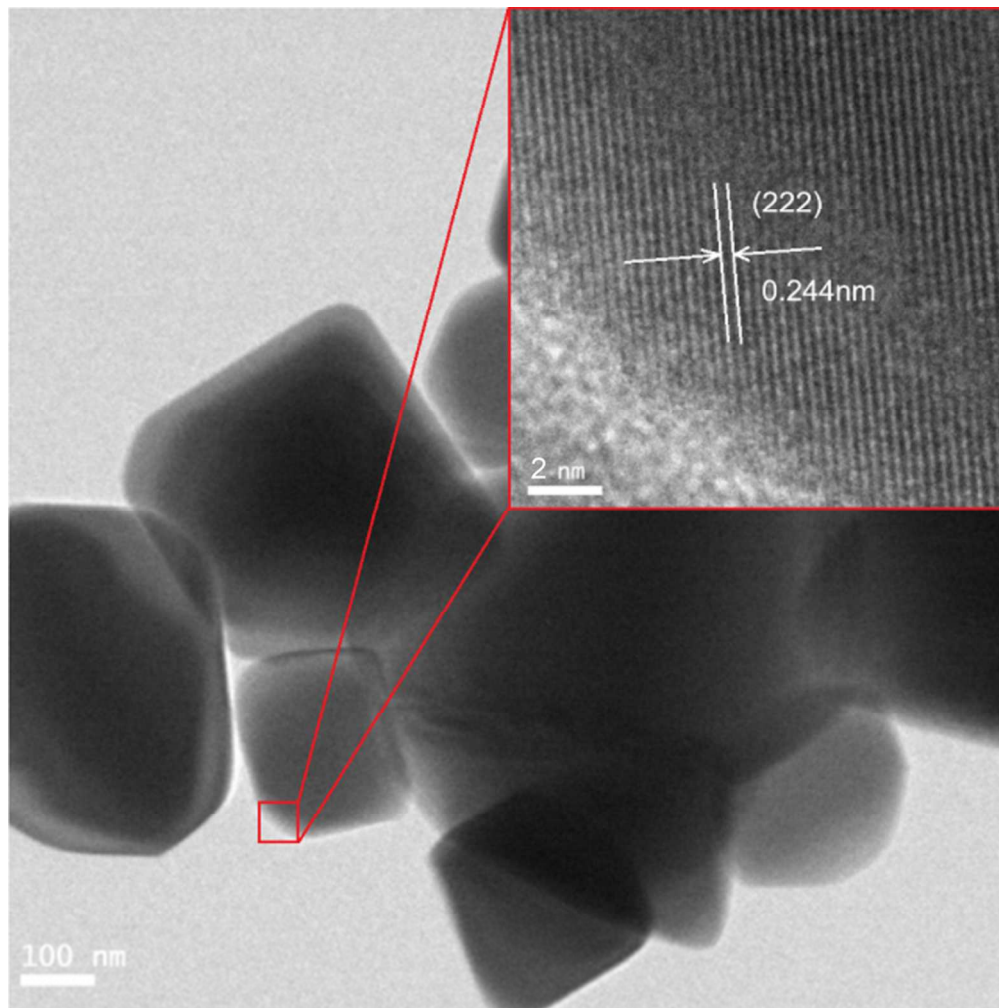


Fig. 5. HRTEM image of $\text{Li}_4\text{Ti}_4.8\text{Fe}_{0.2}\text{O}_{12}$ powder.
83x83mm (300 x 300 DPI)

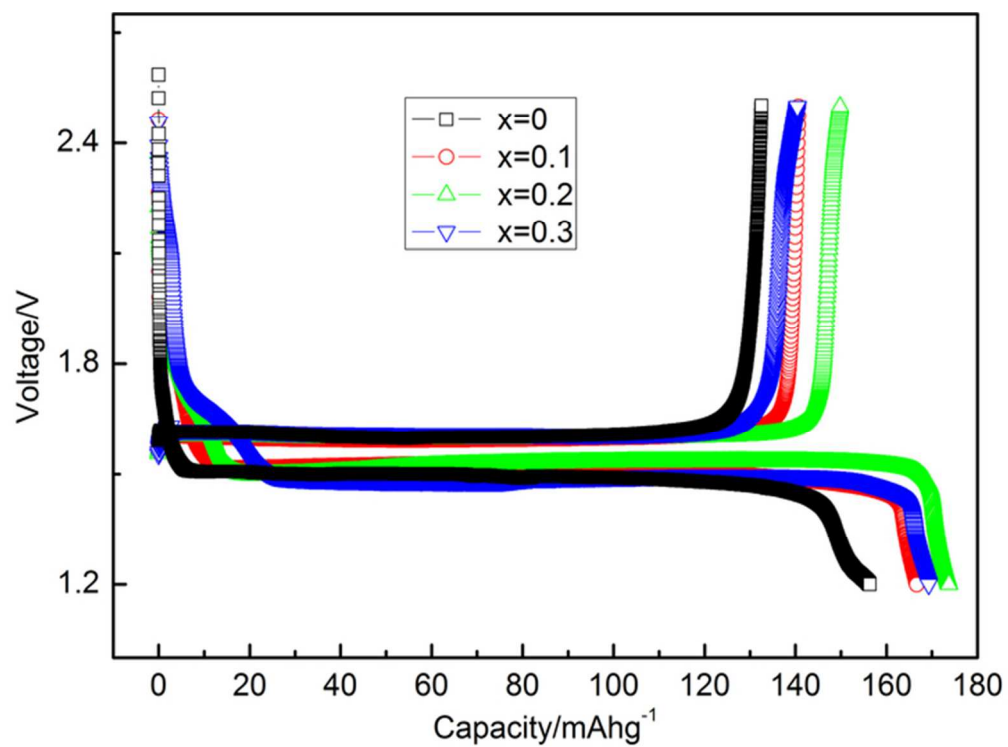


Fig. 6. (a) First charge/discharge curves.
60x44mm (300 x 300 DPI)

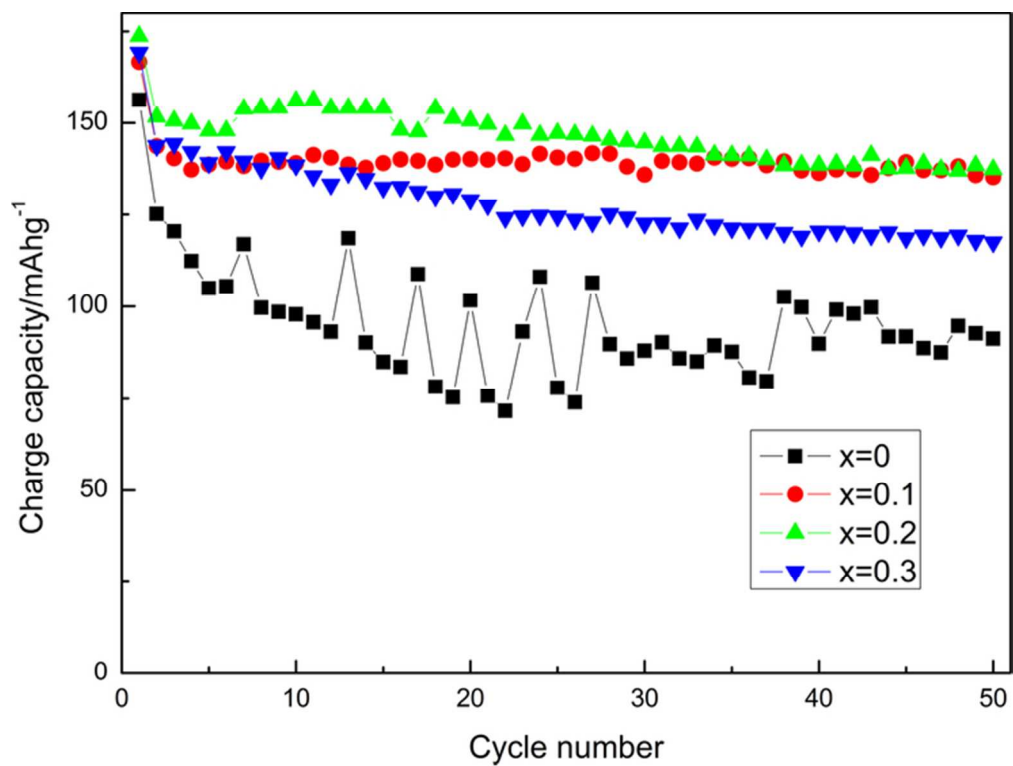


Fig. 6. (b) specific charge capacities at 0.2 C for 50 cycles;
62x47mm (300 x 300 DPI)

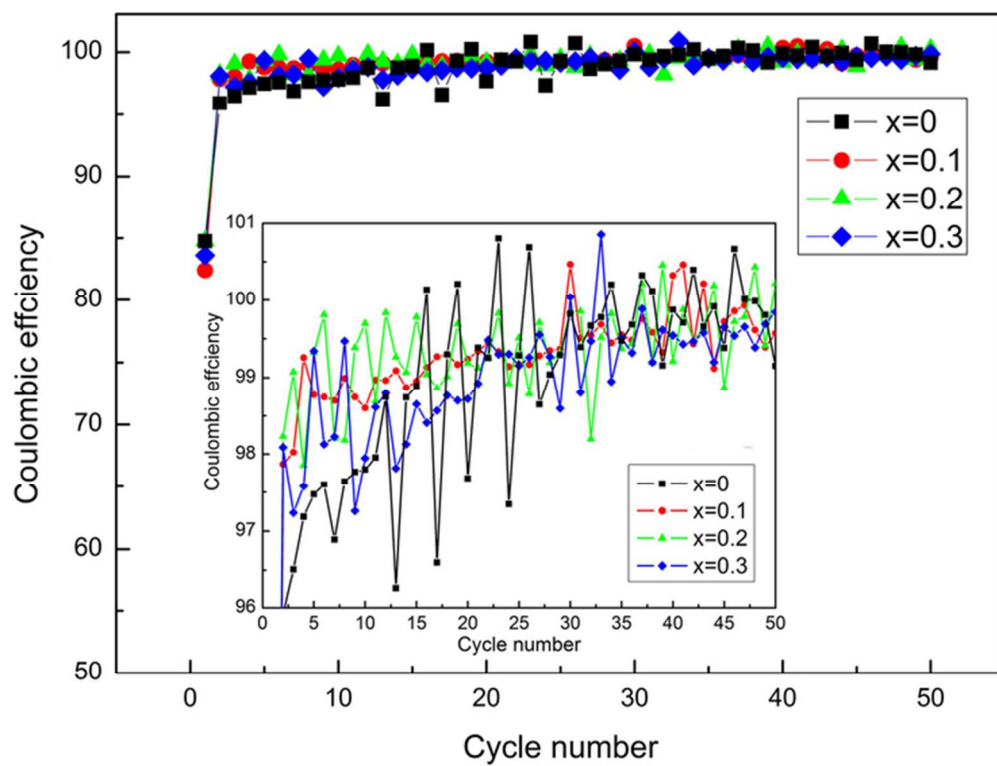


Fig. 6. (c) coulombic efficiency of $\text{Li}_4\text{Ti}_5\text{-xFe}_x\text{O}_{12}$ ($x=0,0.1,0.2,0.3$) at 0.2 C rate between 1.2 and 2.5 V (versus Li/Li+) ;
62x47mm (300 x 300 DPI)

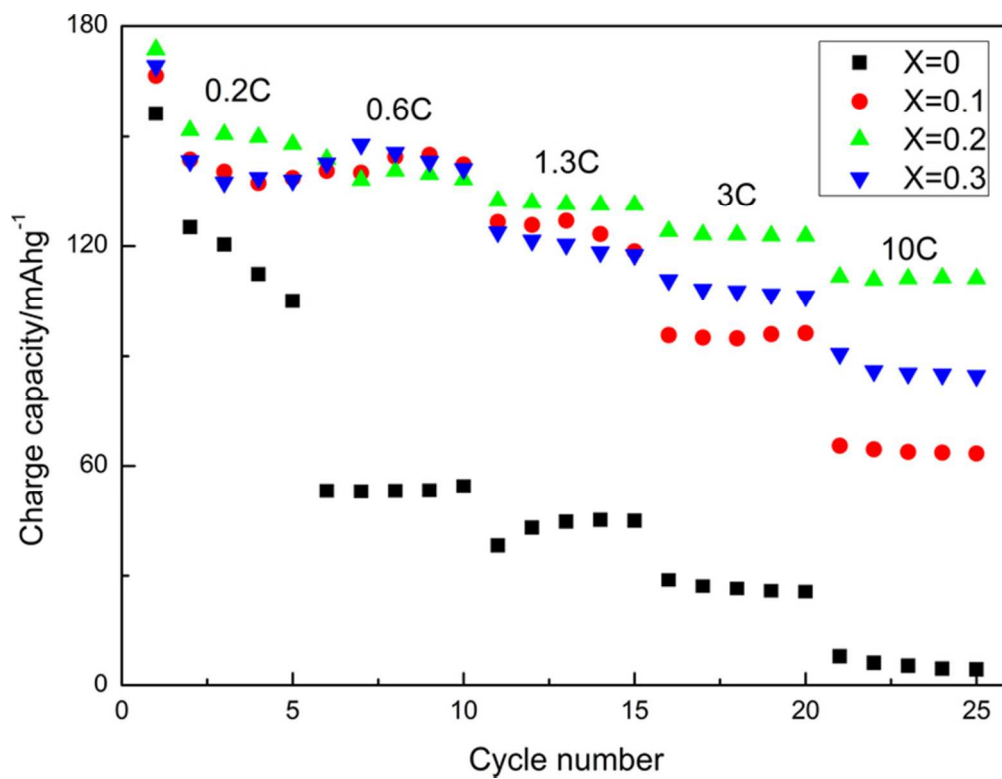


Fig. 6. (d) the rate capabilities of charge at different rates.
63x48mm (300 x 300 DPI)

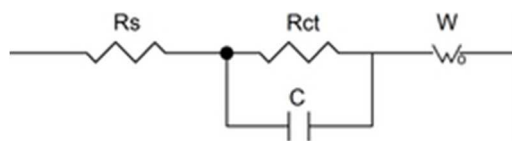


Fig. 7. (b) the equivalent circuit for the EIS.
21x5mm (300 x 300 DPI)

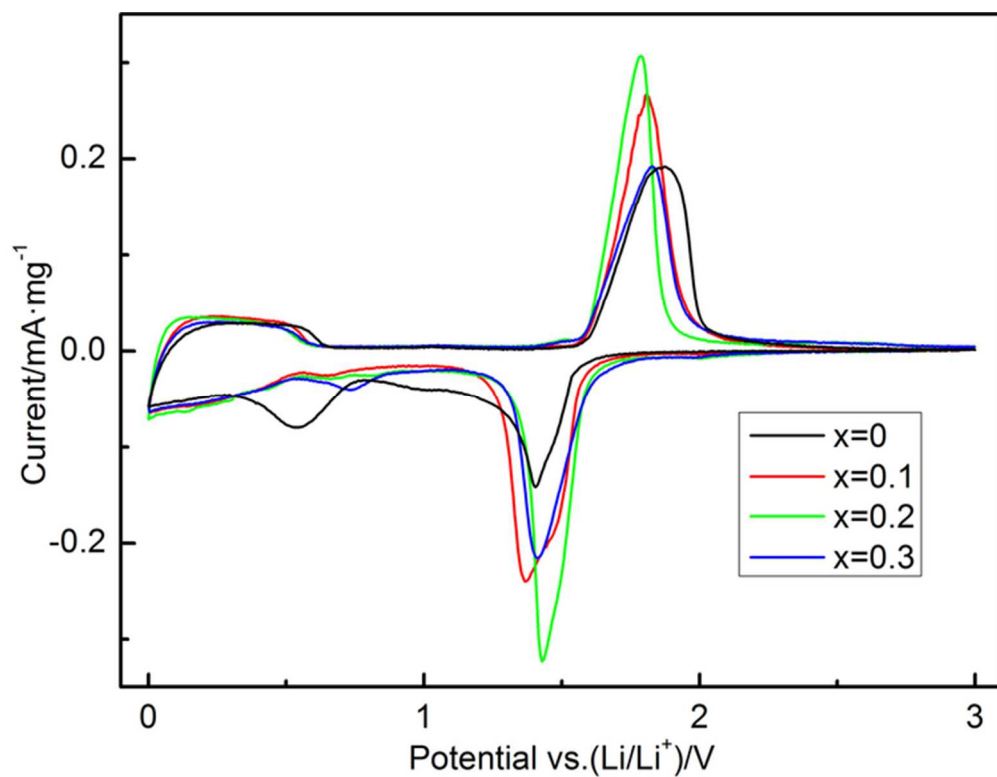


Fig. 8. Cyclic voltammograms of $\text{Li}_4\text{Ti}_5\text{-xFexO}_{12}$ ($x=0,0.1,0.2,0.3$) electrodes in a 1M LiPF₆ in ethylene carbonate (EC), dimethyl carbonate (DMC) and ethyl methyl carbonate (EMC) (1:1:1 in volume) electrolyte with scan rate of 0.1 mV/s. WE: LT(F)O electrodes (1.13 cm²), CE and RE: Li foil (2.01 cm²).
63x48mm (300 x 300 DPI)